AIMS Mathematics, 11(8): 23663–23686.
DOI: 10.3934/math.2026953
Received: 31 January 2026
Revised: 08 May 2026
Accepted: 29 May 2026
Published: 03 August 2026

http://www.aimspress.com/journal/Math

Research article

Vaccination and transmission interplay in HAV-HIV co-infection: A predictive study backed by simulation

Shaiza Irum[1], Kashif Ali Khan[1], Nauman Raza[2], Waleed M. Abdelfattah[3,4], Wedad Albalawi[5], Ahmed M. Shehata[6] and Gamal M. Ismail[7,*]

[1] Department of Mathematics, University of Engineering and Technology, Lahore, Pakistan

[2] Institute of Mathematics, University of the Punjab, Lahore, Pakistan

[3] College of Engineering, University of Business and Technology, Jeddah 23435, Saudi Arabia

[4] Department of Engineering Mathematics and Physics, Faculty of Engineering, Zagazig University, Zagazig 44519, Egypt

[5] Department of Mathematical Sciences, College of Science, Princess Nourah bint Abdulrahman University, P.O. Box 84428, Riyadh 11671, Saudi Arabia

[6] Department of Mathematics, College of Sciences, University of Bisha, Bisha 61922, Saudi Arabia

[7] Department of Mathematics, Faculty of Science, Islamic University of Madinah, Madinah 42351, Saudi Arabia

* **Correspondence:** Email: gismail@iu.edu.sa.

Abstract: This study proposes an epidemiological model for hepatitis A virus (HAV) and human hmmunodeficiency virus (HIV) co-infection in the United States of America, incorporating an integer-order derivative. The model's mathematical properties, including non-negativity and boundedness, are carefully examined and confirmed. Additionally, equilibrium points at the disease-free states are determined, along with the calculation of the reproduction number. With the aid of partial rank correlation coefficient (PRCC) and Latin hypercube sampling (LHS), sensitivity analyses of the basic reproduction numbers are performed using 1200 simulations. Local and global stability of the disease-free equilibrium point are established by employing a Lyapunov function and LaSalle's invariance principle. Using generated HIV and HAV data for the United States from 2014 to 2023, the model reproduces co-infection dynamics, and the MATLAB's built-in routine bvp4c is used to study the effects of vaccination, transmission, and co-infection on both diseases. These results further support the conclusion that if vaccination coverage increases, co-infection may reduce and disease control improves. To this end, these results show important thresholds that concern how disease persists, and highlight the need to research intervention strategies more and allocate targeted resources to control outbreaks.

Keywords: antiretroviral therapy; HAV and HIV co-infection; sensitivity analysis and parameter estimation
Mathematics Subject Classification: 37G35, 37N25

1. Introduction

Hepatitis A virus (HAV) is affiliated with the Picornaviridae family and is a non-enveloped RNA virus that belongs to the genus Hepatovirus [1]. It infects the liver and triggers a short-term inflammatory response that disrupts routine liver activity. It often causes acute hepatitis, which can result in mild or severe liver inflammation [2]. However, hepatitis B (HBV) and hepatitis C (HCV), HAV does not cause chronic infection; nonetheless, it can occasionally cause fulminant hepatitis, particularly in older persons or those with pre-existing liver disease [3]. HAV usually spreads through close contact with an infected person or by eating or drinking food or water that has been contaminated with feces. It is more common in places with bad sanitation [4]. On average, the time takes for it to hatch is 28 days, but it can take anywhere from 15 to 50 days. Typical signs of infection include fever, fatigue, loss of appetite, nausea, vomiting, stomach discomfort, darkened urine, and yellowing of the skin or eyes. The amount of virus in the body rises early in the course of infection and then declines as the immune response develops [5]. HAV can be detected in the bloodstream one to two weeks before symptoms appear. Globally, an estimated 114 million people are infected per year, many without symptoms, while about a million experience noticeable illness [6]. Additionally, recent FAO and WHO data from December 2024 suggest that HAV is responsible for roughly 14 million cases and about $28,000$ deaths annually [7].

After entering human cells, human immunodeficiency virus (HIV) converts its RNA into DNA and inserts this material into the host's genome, allowing the infection to persist. The body's defense system begins to deteriorate by this pattern of illness progression, making people more susceptible to a variety of infections. HIV continues to be a major global health challenge, even with the progress that has been made in treatment [8]. Since the virus first emerged in the early 1980s, nearly 40 million people have died from HIV-related illnesses, and by 2023, around 39 million people were estimated to be living with the infection [9]. HIV is mainly transmitted through unprotected sexual contact, sharing contaminated needles, transfusion of infected blood, and from mother to child during pregnancy, childbirth, or breastfeeding.

The virus is of two principal kinds: HIV-1, which is more common and virulent, and HIV-2 [10]. Once the virus gets into the body, HIV works through a process known as the reverse transcription whereby the virus infects the host cells by inserting its genetic material into their cells, thus being able to fit into the body of a person and stay dormant until a later date when it is activated to cause the disease again [11]. Unattended HIV may develop into AIDS, characterized by a CD4+ cell count of less than 200 cells /mm 3 or the emergence of certain opportunistic infections and malignancies [12].

Although there is still no cure or fully effective vaccine, the use of combination antiretroviral therapy (ART) has greatly improved the management of the disease. Early diagnosis and maintaining long-term viral suppression remain key to controlling HIV at both the individual and global levels [13].

Classical susceptible-infected-recovered (SIR)-based compartmental models are still fundamental

in making predictions of the dynamics of infectious diseases, assessing intervention strategies, and studying threshold behavior. They are mathematically tractable to enable rigorous exploration of stability properties and reproduction numbers, which are vital to public health planning. More recently, to consider memory effects and hereditary properties in the transmission of epidemics, fractional-order extensions have been proposed. As an example, Caputo derivative-based methods have been used to model viral dynamics and incorporate machine learning methods to obtain predictive accuracy, whereas Atangana–Baleanu–Caputo (ABC) fractional operator models have been used to analyze longer susceptible-exposed-infected-recovered (SEIR) systems with memory-dependent transmission behavior. The integer-order models still offer a sound analytical basis despite such innovations, and especially in examining the equilibrium stability, sensitivity analysis, and threshold conditions of co-infection conditions. The current research is created in the classical integer-order framework with references to these new extensions [14–18].

HIV and HAV co-existence is now a significant issue of public health concern, especially in people with weakened immune systems. Even though HAV typically results in a mild illness that is a self-limiting condition in otherwise healthy individuals, it may become more serious in patients living with HIV [19]. HIV suppresses the immune system of the body and thus causes difficulty in combating HAV, which results in prolonged infections, a higher level of liver inflammation, and in uncommon cases, severe hepatitis. HAV outbreaks have been increasingly common in HIV-positive communities in the past years with particular prevalence among injecting drug users and men who have sex with men. This is what complicates treatment, raises healthcare expenses, and makes special preventive actions, including vaccination, early diagnosis, and frequent observation of liver status, significant and necessary foci of prevention of these infections [20].

According to Nagu et al. [21], it was found that about 20 % of HIV-positive individuals were also exposed to HBV or HCV. Since most of them exhibit only mild increases in liver enzyme levels and even no symptoms whatsoever it is particularly necessary to incorporate regular hepatitis screening and adequate management as components of HIV care programs. Serious liver problems might arise when HIV and HBV co-occur with hepatitis C [22]. Liver fibrosis is a result of concurrent infection with HBV and HCV, and as HIV treatment has advanced, the detrimental effects of HCV have become more obvious. Research is still ongoing to determine the best ways to treat these co-infections. HCV and HIV co-infection is more common among drug users, and HIV accelerates the course of HCV [23]. Moreover, the treatment is much more difficult by the possibility of liver damage associated with several HIV drugs. Backus et al. [24] reported that 37% of HIV-positive veterans also had HCV. Many also had to battle with substance abuse and mental health problems. According to Operskalski et al. [25], HCV affects approximately 130 million people globally, of whom four to five million are co-infected with HIV. HIV promotes liver damage; however, it is unknown how HCV affects HIV. Although advances in HIV treatment have enhanced life expectancy, HCV-related liver disease continues to be a major issue.

Moreover, it is necessary to know the effect of variability of the parameters in order to create effective intervention strategies. The rates of transmission and vaccination coverage as well as the rate of treatment progression have a direct impact on the magnitude and persistence of epidemics. The quantitative measure of threshold behavior and control effectiveness is given by assessing the sensitivity of these parameters to changes in the dynamics of a disease. Moreover, classical integer-order models suppose the immediate reaction to epidemiological fluctuations, which might

be unsuitable to depict infections with incubation periods, immune memory, and compound effects of treatments, like HAV and HIV.

In contrast to previous studies, we provide a co-infection framework that evaluates HAV and HIV simultaneously [21–25]. This work advances beyond single-infection models of HAV or HIV by formulating a unified co-infection framework. The analysis makes our study stand out because our model integrates a dedicated HAV vaccination compartment, which gives a clearer picture of how the disease evolves. It combines vaccination, treatment processes, and epidemiological calibration within one framework, rather than treating them separately. We also consider things like waning immunity after vaccination, different routes of co-infection, and how treatment can shift individuals between disease states, allowing for a more realistic assessment of intervention strategies.

To study the model effectively, we performe both qualitative and quantitative analyses, including stability analysis and partial rank correlation coefficient-Latin hypercube sampling (PRCC-LHS) sensitivity methods, and results in detail. We also enrich the study by incorporating real HAV data from the United States, which helps make the results more practical and reliable, while HIV data are synthetically generated. Overall, the study looks at how the disease spreads and what factors influence it, with the aim of supporting better public health decisions. Taken together, these elements make the model a more useful and complete tool for evaluating intervention strategies.

The analysis of this paper is discussed in 11 sections. Section 2 discusses the details of the model establishment. The qualitative analysis like equilibrium points and the reproduction number are examined in Sections 3 and 4, respectively. We discuss the stability analysis in Section 6 and the sensitivity analysis in Section 5. Section 7 explains parameter estimation, and Section 8 covers the numerical study with the results discussed in Section 9. Section 10 covers the conclusions of this study; meanwhile, Section 11 covers the limitations and future works.

2. Model establishment

In this study, the co-infection dynamics of HIV and HAV are described by using eight ordinary differential equations. Table 1 lists the eight exclusive compartments into which $\mathfrak{L}$(t) falls at any given time t. The model's disease dynamics are shown in Figure 1, which maps all variable transitions between compartments and emphasizes their interdependencies. In this study, δ denotes deaths unique to each compartment while the natural death rate is represented by μ. Both of these parameters are essential in shaping population changes and disease spread within the model. Therefore,

$$\mathfrak{L}(t) = S(t) + V(t) + E(t) + H_A(t) + H_V(t) + C(t) + T_V(t) + R(t).$$

The susceptible population grows at a rate η. Individuals transition from S to V at rate θ. Susceptibles are exposed to HAV at rate ϕ and infected with HIV at rate λ_V, given by $\lambda_V = \frac{\alpha_V(H_V(t)+C(t))}{\mathfrak{L}(t)}$, where α_V is the HIV transmission rate. The model also incorporates the natural death rate μ.

$$\frac{dS}{dt} = \eta - \theta S - \lambda_A S - \lambda_V S - \mu S. \tag{2.1}$$

The vaccinated class receives HAV immunization at rate θ. They move to the exposed class at $(1 - \epsilon)$, with the equation also accounting for the natural death rate μ.

$$\frac{dV}{dt} = \theta S - (1 - \epsilon)\lambda_A V - \mu V. \tag{2.2}$$

The exposed class arises from vaccination at $(1-\epsilon)$ and susceptibility at ϵ. Individuals progress to infection at λ_A, where $\lambda_A = \frac{\alpha_A(H_A(t)+C(t)}{\Omega(t)}$ is the transmission rate of HAV, and some move to the recovery class at γ_1. As they do not transmit the pathogen, the natural death rate μ applies.

$$\frac{dE}{dt} = (1-\epsilon)\lambda_A V + \lambda_A S - (\phi + \gamma_1 + \mu)E. \tag{2.3}$$

The infected HAV class results from exposed individuals becoming infected. Some transition to the co-infection class at rate λ_V, while others recover at γ_2. The death rate in this case is $(\mu + \delta_1)$ due to infection.

$$\frac{dH_A}{dt} = \phi E - \lambda_V H_A - (\gamma_2 + \mu + \delta_1)H_A. \tag{2.4}$$

Table 1. Model variable categorization.

Variable	Description
S	Susceptible individuals
V	HAV vaccinated individuals
E	Individuals exposed with HAV
H_A	HAV infected individuals
H_V	HIV infected individuals
C	Co-infected individuals
T_V	Treated HIV individuals
R	HAV recovered individuals

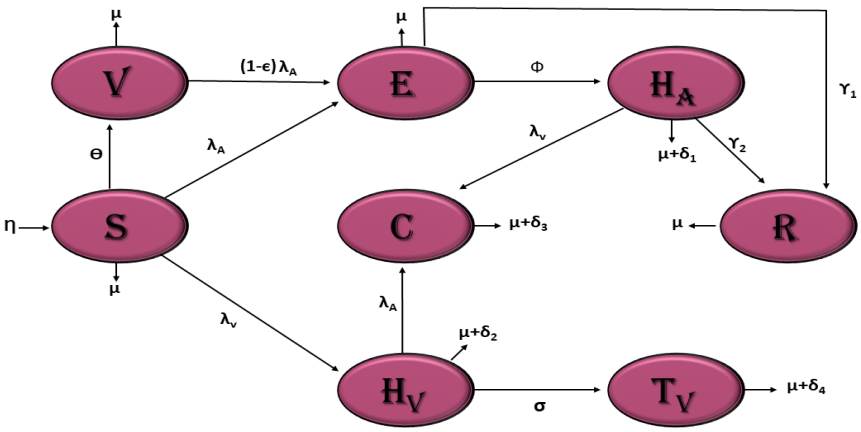

Figure 1. Flowchart illustrating HAV and HIV co-infection transmission.

The infected HIV class arises as susceptibles contract HIV. Some move to the co-infection class at λ_V, while others enter treatment at σ. Though treatment aids recovery, it is not always effective cause

there has been no treatment for HIV till today, yet ART is very effective. The death rate is $(\mu + \delta_2)$,

$$\frac{dH_V}{dt} = \lambda_V S - \lambda_A H_V - (\sigma + \mu + \delta_2)H_V. \tag{2.5}$$

The co-infected population grows as HAV-infected individuals get HIV at λ_V and HIV-infected individuals acquire HAV at λ_A, while it declines due to mortality at $(\mu + \delta_3)$,

$$\frac{dC}{dt} = \lambda_V H_A + \lambda_A H_V - (\mu + \delta_3)C. \tag{2.6}$$

The treated HIV population grows at σ and declines due to mortality at $(\mu + \delta_4)$,

$$\frac{dT_V}{dt} = \sigma H_V - (\mu + \delta_4)T_V. \tag{2.7}$$

The recovery population grows at $(\gamma_1 + \gamma_2)$ and declines at μ,

$$\frac{dR}{dt} = \gamma_1 E + \gamma_2 H_A - \mu R. \tag{2.8}$$

By combining the equations from (2.1) to (2.8), we derive a system that models HAV-HIV dynamics, capturing susceptibility, infection, treatment, and recovery processes.

$$\left\{\begin{array}{l} \frac{dS}{dt} = \eta - \theta S - \lambda_A S - \lambda_V S - \mu S, \\ \frac{dV}{dt} = \theta S - (1-\epsilon)\lambda_A V - \mu V, \\ \frac{dE}{dt} = (1-\epsilon)\lambda_A V + \lambda_A S - (\phi + \gamma_1 + \mu)E, \\ \frac{dH_A}{dt} = \phi E - \lambda_V H_A - (\gamma_2 + \mu + \delta_1)H_A, \\ \frac{dH_V}{dt} = \lambda_V S - \lambda_A H_V - (\sigma + \mu + \delta_2)H_V, \\ \frac{dC}{dt} = \lambda_V H_A + \lambda_A H_V - (\mu + \delta_3)C, \\ \frac{dT_V}{dt} = \sigma H_V - (\mu + \delta_4)T_V, \\ \frac{dR}{dt} = \gamma_1 E + \gamma_2 H_A - \mu R. \end{array}\right\} \tag{2.9}$$

The system begins with the following initial conditions:

$$\begin{array}{c} S(t) > 0,\ V(t) \geq 0,\ E(t) \geq 0,\ H_A(t) \geq 0, \\ H_V(t) \geq 0,\ C(t) \geq 0,\ T_V(t) \geq 0,\ R(t) \geq 0. \end{array} \tag{2.10}$$

The following region is designated for studying the model system (2.9) based on biological reasoning

$$\mathcal{A} = \left\{(S, V, E, H_A, H_V, C, T_V, R) \in \mathrm{R}_+^8 : \mathfrak{L} \leqslant \frac{\eta}{\mu}\right\}, \tag{2.11}$$

which upholds positive invariance under the dynamics of model system (2.9).

Theorem 2.1. *The model system (2.9) admits a unique solution $\nu = (S, V, E, H_A, H_V, C, T_V, R)$ that meets the initial conditions specified in (2.10) within the positive region $\mathcal{A}$.*

Proof. To establish the positive invariance of region $\mathcal{A}$ in Eq (2.11), it must be proven that any solution initiating in $\mathcal{A}$ remains within the region for all $t \geqslant 0$. To begin, we observe that the trajectory remains

confined within $\mathcal{A}$ as t increases, which is crucial for ensuring positive invariance. Initially, we note that

$$\begin{aligned}
\left.\frac{dS}{dt}\right|_{S=0} &= \eta > 0,\\
\left.\frac{dV}{dt}\right|_{V=0} &= \theta S \geqslant 0,\\
\left.\frac{dE}{dt}\right|_{E=0} &= (1-\epsilon)\lambda_A V + \lambda_A S \geqslant 0,\\
\left.\frac{dH_A}{dt}\right|_{H_A=0} &= \phi E \geqslant 0,\\
\left.\frac{dH_V}{dt}\right|_{H_V=0} &= \lambda_V S \geqslant 0,\\
\left.\frac{dC}{dt}\right|_{C=0} &= \lambda_V H_A + \lambda_A H_V \geqslant 0,\\
\left.\frac{dT_V}{dt}\right|_{T_V=0} &= \sigma H_V \geqslant 0,\\
\left.\frac{dR}{dt}\right|_{R=0} &= \gamma_1 E + \gamma_2 H_A \geqslant 0.
\end{aligned}$$

To ensure the solution components remain bounded, we examine the total population dynamics within the structure of system (2.9),

$$\frac{d\mathfrak{L}}{dt} = \eta - \mu\mathfrak{L}(t) - (\delta_1 H_A + \delta_2 H_V + \delta_3 C + \delta_4 T_V) \leqslant \eta - \mu\mathfrak{L}(t).$$

If $\mathfrak{L}(0) < \mu$, then $\mathfrak{L}(t)$ remains within $0 < \mathfrak{L}(t) < \mu$ for all $t \geqslant 0$. This verifies that the entire population $\mathfrak{L}(t)$ remains within the range ranging from 0 to μ, proving the boundedness of all aspects of the solution and retaining the model inside its set boundaries. Therefore, the area defined by $\mathcal{A}$ is positively invariant, and each route of the mathematical system stays within this set for all subsequent periods. □

Theorem 2.2. *All solutions of the nonlinear system (2.9) stay restricted to the bounded region defined in (2.11).*

Proof. Through the system (2.9), we can define a region in which every solution of the system remains bounded. In simple terms, it means the population values stay realistic; they don't shoot off to infinity or fall below zero, so the model continues to make practical sense.

$$\mathfrak{L}(t) = S(t) + V(t) + E(t) + H_A(t) + H_V(t) + C(t) + T_V(t) + R(t),$$

$$\frac{\mathfrak{L}(t)}{dt} = \frac{dS(t)}{dt} + \frac{dV(t)}{dt} + \frac{dE(t)}{dt} + \frac{dH_A(t)}{dt} + \frac{dH_V(t)}{dt} + \frac{dC(t)}{dt} + \frac{dT_V(t)}{dt} + \frac{dR(t)}{dt},$$

$$\frac{d\mathfrak{L}}{dt} = \eta - \mu\mathfrak{L}(t) - (\delta_1 H_A + \delta_2 H_V + \delta_3 C + \delta_4 T_V),$$

$$\frac{d\mathfrak{L}}{dt} \leqslant \eta - \mu\mathfrak{L}(t). \tag{2.12}$$

Equation (2.12) undergoes the Laplace transform, yielding in

$$s\mathfrak{L}(s) - \mathfrak{L}(0) \leqslant \frac{\eta}{s} - \mu\mathfrak{L}(s),$$

$$(s+\mu)\mathfrak{L}(s) \leqslant \frac{\eta}{s} + \mathfrak{L}(0),$$

$$\mathfrak{L}(s) \leqslant \frac{\eta}{s(s+\mu)} + \frac{\mathfrak{L}(0)}{(s+\mu)},$$

$$\mathfrak{L}(s) \leqslant \frac{\eta}{\mu s} - \frac{\eta}{\mu(\mu+s)} + \frac{\mathfrak{L}(0)}{(\mu+s)},$$

$$\mathfrak{L}(t) \leqslant \frac{\eta}{\mu} + \left\{\mathfrak{L}(0) - \frac{\eta}{\mu}\right\}e^{-\mu t}.$$

As $t \to \infty$, $e^{-\mu t}$ vanishes, resulting in $\mathfrak{L}(t) \to \frac{\eta}{\mu}$. Hence,

$$\lim_{t\to\infty} \mathfrak{L}(t) \to \frac{\eta}{\mu}.$$

□

3. Equilibrium points

By evaluating the framework in (2.9), we find the framework's states of equilibrium, which capture both the healthy state and the disease-causing state. There are no pathogens at the disease-free equilibrium, which halts the transmission of illness. This state plays a crucial role in controlling and analyzing transmission thresholds. Thus, we consider $E = 0, H_A = 0, H_V = 0, C = 0, T_V = 0$, and $R = 0$ in the system (2.9). The disease-free equilibrium point $\mathcal{D}^0$ is determined as:

$$\mathcal{D}^0 = (S^0, V^0, E^0, H_A^0, H_V^0, C^0, T_V^0, R^0) = \left(\frac{\eta}{\theta+\mu}, \frac{\eta\theta}{\mu(\theta+\mu)}, 0, 0, 0, 0, 0, 0\right).$$

4. Reproduction number

In a fully vulnerable population, the fundamental reproduction number, $\mathcal{R}_0$, calculates the average number of new infections brought on by a single sick person [26, 27]. When $\mathcal{R}_0 > 1$, the disease spreads, as each infected person transmits the infection to more than one individual before recovering. Conversely, if $\mathcal{R}_0 < 1$, the outbreak declines, as each infected individual transmits the disease to fewer than one person on average. To determine $\mathcal{R}_0$, the next-generation matrix method [28] is used. This method uses the spectral radius of the matrix FV^{-1} to figure out the disease impact. Below F represents the new infection in the framework, and V describes the transition rates within the compartmental framework.

$$F = \begin{pmatrix} 0 & \alpha_A - \frac{\alpha_A\theta\epsilon}{\theta+\mu} & 0 & \alpha_A - \frac{\alpha_A\theta\epsilon}{\theta+\mu} & 0 \\ 0 & 0 & 0 & 0 & 0 \\ 0 & 0 & \frac{\alpha_V\mu}{\theta+\mu} & \frac{\alpha_V\mu}{\theta+\mu} & 0 \\ 0 & 0 & 0 & 0 & 0 \\ 0 & 0 & 0 & 0 & 0 \end{pmatrix}, \quad V = \begin{pmatrix} m_1 & 0 & 0 & 0 & 0 \\ -\phi & m_2 & 0 & 0 & 0 \\ 0 & 0 & m_3 & 0 & 0 \\ 0 & 0 & 0 & m_4 & 0 \\ 0 & 0 & -\sigma & 0 & m_5 \end{pmatrix},$$

$$V^{-1} = \begin{pmatrix} \frac{1}{m_1} & 0 & 0 & 0 & 0 \\ \frac{\phi}{m_1 m_2} & \frac{1}{m_2} & 0 & 0 & 0 \\ 0 & 0 & \frac{1}{m_3} & 0 & 0 \\ 0 & 0 & 0 & \frac{1}{m_4} & 0 \\ 0 & 0 & \frac{\sigma}{m_3 m_5} & 0 & \frac{1}{m_5} \end{pmatrix}, \quad FV^{-1} = \begin{pmatrix} 0 \\ 0 \\ 0 \\ \frac{\alpha_V \mu}{m_3(\theta+\mu)} \\ \frac{\alpha_A \phi\,(\theta+\mu+\theta(1-\epsilon))}{m_1 m_2(\theta+\mu)} \end{pmatrix},$$

where,

$$m_1 = \phi + \gamma_1 + \mu,\ m_2 = \gamma_2 + \mu + \delta_1,\ m_3 = \sigma + \mu + \delta_2,\ m_4 = \mu + \delta_3,\ m_5 = \mu + \delta_4.$$

Hence, the basic reproduction number $\mathcal{R}_0 = \max(\mathcal{R}_V, \mathcal{R}_A)$ is determined as the largest eigenvalue of the matrix product FV^{-1}. The reproduction numbers of HAV and HIV are represented by $\mathcal{R}_V$ and $\mathcal{R}_A$. Sensitivity analysis of $\mathcal{R}_0$ indicates that strengthening vaccination efforts (θ) and improving treatment access (σ) can effectively restrain disease transmission, while higher transmission coefficients (α_V, α_A) escalate outbreak severity. To simply summarize, increasing vaccine uptake biologically constrains the susceptible pool and suppresses HAV spread.

5. Sensitivity analysis

Sensitivity analysis PRCC-LHS to evaluate how parameter changes affect the suggested HIV model [29]. Finding the most sensitive parameters is crucial since changes in their numerical values can have a big impact on the dynamics of the model. Sensitivity analysis assists in determining critical factors that are essential for lowering $\mathcal{R}_0$ and limiting the spread of disease. The most powerful people have high PRCC scores. Figure 2 illustrates the PRCC scores associated with each parameter. They are crucial in the progession of the disease. From the graph, we can see the parameters. α_V has the strongest positive effect; meanwhile, θ and σ contribute notably. These values directly affect $\mathcal{R}_0$ as this plays a crucial role in curbing the disease.

Figure 3a displays a contour plot that illustrates how varying values of α_V and θ impact $\mathcal{R}_0$, with lighter shades indicating higher values. As soon as $\mathcal{R}_0$ increases the system tends to move toward the endemic state. To give a clearer sense of this relationship, Figure 3b adds a 3D surface view, making it easier to see how $\mathcal{R}_0$ changes as both parameters vary together. Taken together, these figures help simplify the interpretation of parameter effects and support decisions aimed at controlling the spread of infection. In Figure 3c, the contour plot shows a clear decrease in $\mathcal{R}_0$ as both σ and θ increase, with values gradually dropping from the lower-left to the upper-right region of the graph. This pattern suggests that increasing either of these parameters helps reduce $\mathcal{R}_0$, which supports strategies aimed at limiting disease transmission. The 3D surface in Figure 3d demonstrates the same trend. As the values of σ and θ rise, $\mathcal{R}_0$ steadily declines, reinforcing the relationship observed in the contour plot.

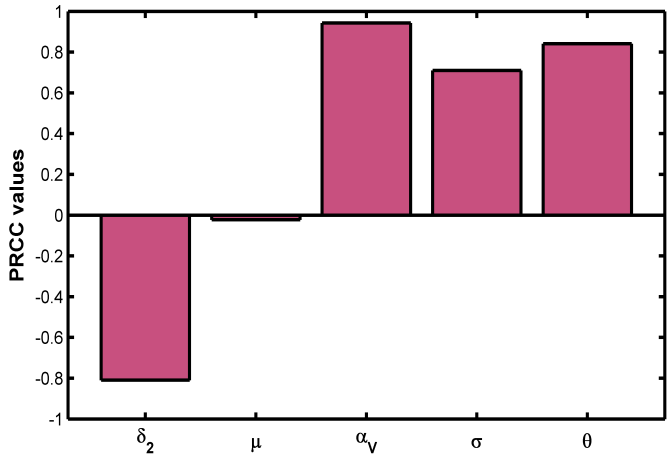

Figure 2. Sensitivity analysis of HIV and HAV co-infection.

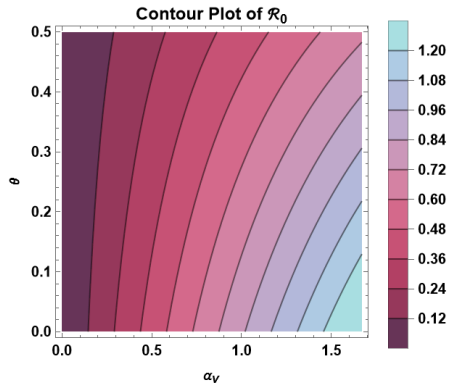

(a) Contour plot of $\mathcal{R}_0$ vs. α_V and θ.

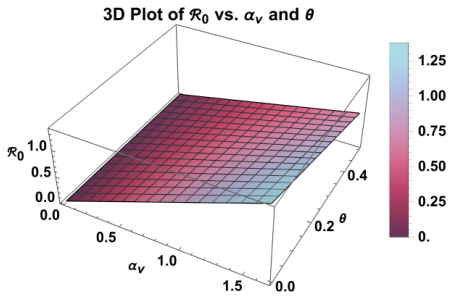

(b) 3-D plot of $\mathcal{R}_0$ vs. α_V and θ.

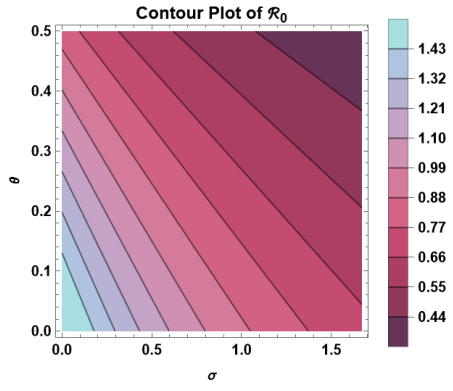

(c) Contour plot of $\mathcal{R}_0$ vs. θ and σ.

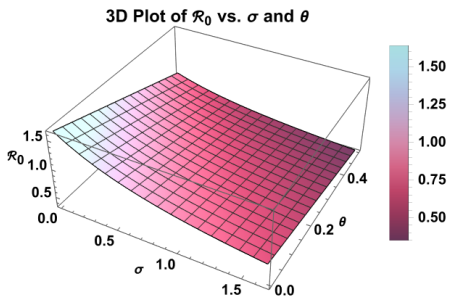

(d) 3-D plot of $\mathcal{R}_0$ vs. θ and σ.

Figure 3. Contours graphs and their 3D representation.

6. Stability analysis

To asses the stability of our framework, we imploy Lyapunov-based techniques. This analysis helps to show how the model behaves in the long run and also pinpoints the scenarios and conditions under which the infection subsides [30].

6.1. Local stability

Theorem 6.1. *For $\mathcal{R}_0 < 1$, the disease-free equilibrium $\mathcal{D}^0$ remains locally asymptotically stable, but it loses stability when $\mathcal{R}_0 \geqslant 1$.*

Proof. The Jacobian matrix $\mathcal{J}(B^0)$ at the disease-free equilibrium $\mathcal{D}^0$ for model (2.9) is computed as follows, offering insights into the system's stability.

$$\mathcal{J}(B^0) = \begin{pmatrix} -\theta-\mu & 0 & 0 & -\frac{\alpha_A\eta}{(\theta+\mu)\left(\frac{\eta}{\theta+\mu}+\frac{\eta\theta}{\mu(\theta+\mu)}\right)} & -\frac{\alpha_V\eta}{(\theta+\mu)\left(\frac{\eta}{\theta+\mu}+\frac{\eta\theta}{\mu(\theta+\mu)}\right)} & -\frac{\alpha_A\eta+\alpha_V\eta}{(\theta+\mu)\left(\frac{\eta}{\theta+\mu}+\frac{\eta\theta}{\mu(\theta+\mu)}\right)} & 0 & 0 \\ \theta & -\mu & 0 & -\frac{\alpha_A\eta\theta(1-\epsilon)}{\mu(\theta+\mu)\left(\frac{\eta}{\theta+\mu}+\frac{\eta\theta}{\mu(\theta+\mu)}\right)} & 0 & -\frac{\alpha_A\eta\theta(1-\epsilon)}{\mu(\theta+\mu)\left(\frac{\eta}{\theta+\mu}+\frac{\eta\theta}{\mu(\theta+\mu)}\right)} & 0 & 0 \\ 0 & 0 & -m_1 & \frac{\alpha_A\eta}{(\theta+\mu)\left(\frac{\eta}{\theta+\mu}+\frac{\eta\theta}{\mu(\theta+\mu)}\right)}+\frac{\alpha_A\eta\theta(1-\epsilon)}{\mu(\theta+\mu)\left(\frac{\eta}{\theta+\mu}+\frac{\eta\theta}{\mu(\theta+\mu)}\right)} & 0 & \text{same} & 0 & 0 \\ 0 & 0 & \phi & -m_2 & 0 & 0 & 0 & 0 \\ 0 & 0 & 0 & 0 & \frac{\alpha_V\eta}{(\theta+\mu)\left(\frac{\eta}{\theta+\mu}+\frac{\eta\theta}{\mu(\theta+\mu)}\right)}-m_3 & \frac{\alpha_V\eta}{(\theta+\mu)\left(\frac{\eta}{\theta+\mu}+\frac{\eta\theta}{\mu(\theta+\mu)}\right)} & 0 & 0 \\ 0 & 0 & 0 & 0 & 0 & -m_4 & 0 & 0 \\ 0 & 0 & 0 & 0 & \sigma & 0 & -m_5 & 0 \\ 0 & 0 & \gamma_1 & \gamma_2 & 0 & 0 & 0 & -\mu \end{pmatrix}.$$

The disease-free equilibrium remains locally asymptotically stable (LAS) if all eigenvalues possess negative real parts. The corresponding characteristic equation is:

$$\frac{(\lambda+\mu)^2(\lambda+m_4)(\lambda+m_5)(\theta+\lambda+\mu)\left[\mu(-\alpha_V+\lambda+m_3)+\theta(\lambda+m_3)\right]\left[\alpha_A\phi\left(\theta(\epsilon-1)-\mu\right)+(\theta+\mu)(\lambda+m_1)(\lambda+m_2)\right]}{(\theta+\mu)^2} = 0. \tag{6.1}$$

The model's six eigenvalues are given by

$$\lambda_1 = -m_4, \quad \lambda_2 = -m_5, \quad \lambda_3 = -(\mu+\theta), \quad \lambda_{4,5} = -\mu, \quad \lambda_6 = \frac{\alpha_V\mu - m_3(\theta+\mu)}{\theta+\mu}.$$

The remaining eigenvalues of the matrix can be determined by employing the characteristic equations.

$$\lambda^2 + a_1\lambda + a_2 = 0, \tag{6.2}$$

where

$$a_1 = \frac{(m_1+m_2)}{(\theta+\mu)}, a_2 = \frac{m_1m_2\left(\alpha_A\phi(\theta(\epsilon-1)-\mu)+(\theta+\mu)(\lambda+m_1)(\lambda+m_2)\right)}{(\theta+\mu)\left(\alpha_A\phi(\theta(\epsilon-1)-\mu)+m_1m_2(\theta+\mu)\right)}(R_0-1). \tag{6.3}$$

It is evident from the equations above that a_1 is a positive value. Additionally, the coefficients remain positive when $R_0 < 1$. The application of the previously mentioned coefficients clearly satisfies the Routh–Hurwitz criteria for a second-order polynomial. Consequently, model (2.9) continues to exhibit local asymptotic stability at the disease-free equilibrium, provided that $R_0 < 1$. This completes the proof. □

6.2. Global stability

Theorem 6.2. *For $\mathcal{R}_0 < 1$, the disease-free equilibrium $\mathcal{D}^0$ in model (2.9) is globally asymptotically stable; otherwise, instability occurs.*

Proof. We construct a Lyapunov function to verify the global asymptotic stability of model (2.9),

$$\mathbf{F}(t) = u_1E + u_2H_A + u_3H_V + u_4C + u_5T_V, \tag{6.4}$$

where

$$u_1 = \frac{\phi}{m_1m_2}, u_2 = \frac{1}{m_2}, u_3 = \frac{1}{m_3}, u_4 = 0, u_5 = 0.$$

Taking the time derivative of (6.4).

$$\begin{aligned}
\frac{d\mathbf{F}(t)}{dt} &= u_1\frac{dE}{dt} + u_2\frac{dH_A}{dt} + u_3\frac{dH_V}{dt} + u_4\frac{dC}{dt} + u_5\frac{dT_V}{dt} \\
&= u_1\Big((1-\epsilon)\lambda_AV + \lambda_AS - m_1E\Big) + u_2\Big(\phi E - \lambda_VH_A - m_2H_A\Big) + u_3\Big(\lambda_VS - \lambda_AH_V - m_3H_V\Big) \\
&\quad + u_4\Big(\lambda_AH_V + \lambda_VH_A - m_4C\Big) + u_5\Big(\sigma H_V - (\mu+\delta_4)T_V\Big), \\
\frac{d\mathbf{F}(t)}{dt} &= u_1\Big((1-\epsilon)\frac{\alpha_AH_A + C}{\mathfrak{Q}}V^0 + \frac{\alpha_AH_A + C}{\mathfrak{Q}}S^0 - m_1E\Big) \\
&\quad + u_2\Big(\phi E - m_2H_A\Big) + u_3\Big(\frac{\alpha_VH_V + C}{\mathfrak{Q}}S^0 - m_3H_V\Big), \\
\frac{d\mathbf{F}(t)}{dt} &\leq (u_1m_1 + u_2m_2)\,E + \left(u_1(1-\epsilon)\frac{\alpha_A}{\eta/\mu}\cdot\frac{\eta\theta}{\mu(\theta+\mu)} + \frac{\alpha_A}{\eta/\mu}\cdot\frac{\eta}{\theta+\mu} - u_2m_2\right)H_A + u_3\left(\frac{\alpha_V}{\eta/\mu} - u_3m_3\right)H_V \\
&\leq H_A(R_A - 1) + H_V(R_V - 1).
\end{aligned}$$

Since all model parameters, transmission rates, and state variables are nonnegative, $\mathbf{F}(t)$ is nonincreasing, satisfying $\frac{d\mathbf{F}(t)}{dt} \leqslant 0$ for $\mathcal{R}_0 = \max(\mathcal{R}_V, \mathcal{R}_A) \leqslant 1$. Equality, which holds only if $E = H_A = H_V = C = T_V = 0$, is among the most famous mathematical states globally. The system stabilizes this state due to its fascination with the way stability appears on the invariant region $\mathcal{A}$. The model involves a disease-free state of a system, and the suitable Lyapunov function $\mathbf{F}$ reflects the researcher's idea of the connection between LaSalle's invariance principle [31] and the vanishing of state variables as t approaches to infinity. The excellent and beautiful model (2.9) contains various elements of art, such as $\mathcal{R}_0 \leqslant 1$, as well as the principles of, for instance, infection elimination and system stability. Figure 4 shows the model's simulation results for $\mathcal{R}_0 < 1$ with different initial conditions. □

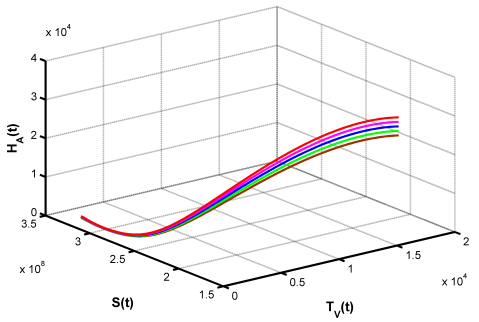

(a) $H_A(t)$ vs. $E(t)$ vs. $V(t)$.

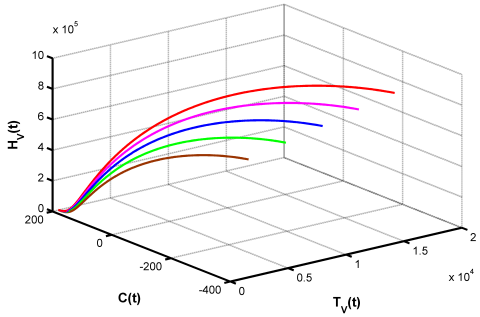

(b) $H_A(t)$ vs. $S(t)$ vs. $T_V(t)$.

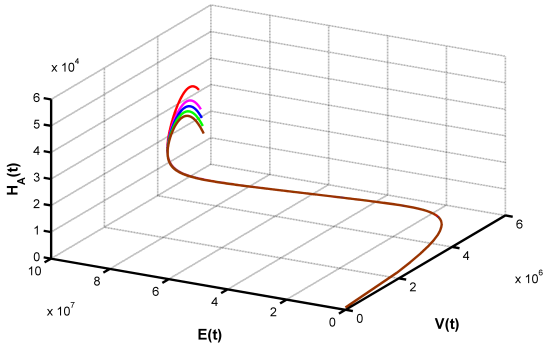

(c) $H_V(t)$ vs. $C(t)$ vs. $T_V(t)$.

Figure 4. Simulated dynamics of infected classes for $\mathcal{R}_0 < 1$ under different initial conditions.

7. Parameter estimation derived from real-world data in the United States

The HAV-HIV co-infection model, adopted in this study, is among the most essential hybrid parameter estimations in epidemiological research. The researchers developed the model due to the limited availability of reliable HAV-HIV co-infection datasets. The study involves real-world HAV incidence data from the United States, and the parameters from existing literature reflect the researchers' idea of the connection between qualitative dynamics and interaction effects. The rigorous and functional HAV-HIV model contains various elements of data, such as HAV incidence, HIV transmission, and co-infection dynamics, as well as the principles of, for instance, biologically feasible ranges and interaction effects.

For the purpose of validating the model, comprehending control strategies, monitoring disease trends, and forecasting epidemics, an accurate estimation of model parameters such as transmission, recovery, mortality, and exposure rates is crucial. The HAV dataset was obtained from the Centers for Disease Control and Prevention (CDC) [32] in the United States. However, owing to the lack of accessible and consistent HIV data for the study population, a synthetic HIV dataset was generated. The generated data were informed by established epidemiological parameters and trends reported in the literature, and were used solely for model calibration and illustrative simulation. While this approach enables the exploration of the model dynamics, the results related to HIV should be interpreted with appropriate caution. The model was fitted to the infection data using MATLAB based on the parameters

in Table 2, and the data offers insights into the course of HAV. By reducing the squared discrepancies between the observed data and model predictions, the least squares method was used to estimate the model parameters. The optimization problem is defined as

$$\min_{\zeta} \sum_{i=1}^{n} \left(I_{\text{data}}(t_i) - I_{\text{model}}(t_i, \zeta)\right)^2 ,$$

where n represents the number of time points and ζ is for the parameters that are selected for optimal calibration. With predetermined starting values and lower boundaries for the parameters, the "lsqcurvefit" function optimized the model. There are 323 million people living there, and the natural death rate is 79 million [26]. We compared the model's predictions with the real infection data shown in Figure 5a after determining the ideal parameters. To assess the model's precision, we calculated the residuals, which are presented in Figure 5b, showing the gaps between observed data and model predictions.

All parameters were adjusted to indicate annual dynamics. The labeled "fitted" parameters were found by applying nonlinear least squares algorithms to CDC surveillance data, meanwhile, the recruitment and death parameters were found by using the known population satistics, which were verified by data on the population of the United States of America [26]. The values termed as fitted were optimized to reduce the error between predicted trends and the recorded figures of infections.

Table 2. Classification of variables used in the model.

Variable	Description	Values per years	Source
η	Recruitment rate	$\frac{323115377}{79}$	[26]
θ	HAV vaccination rate	0.133467	Fitted
μ	Natural death rate	1/79	[26]
ϕ	HAV E to H_A	0.088277	Estimated
α_V	HIV transmission rate	0.149726	Estimated
α_A	HAV transmission rate	0.879999	Estimated
σ	Progression rate of H_V to T_V	0.001000	Estimated
γ_1	Recovery rate of E	0.28	Fitted
γ_2	Recovery rate of H_A	0.327	Fitted
ϵ	Rate V to E	0.690000	Estimated
δ_1	Death rate associated to H_A	0.005	Fitted
δ_2	Death rate of H_V	0.002	Fitted
δ_3	Death rate associated with C	0.001	Fitted
δ_4	Death rate associated with T_V	0.02	Fitted

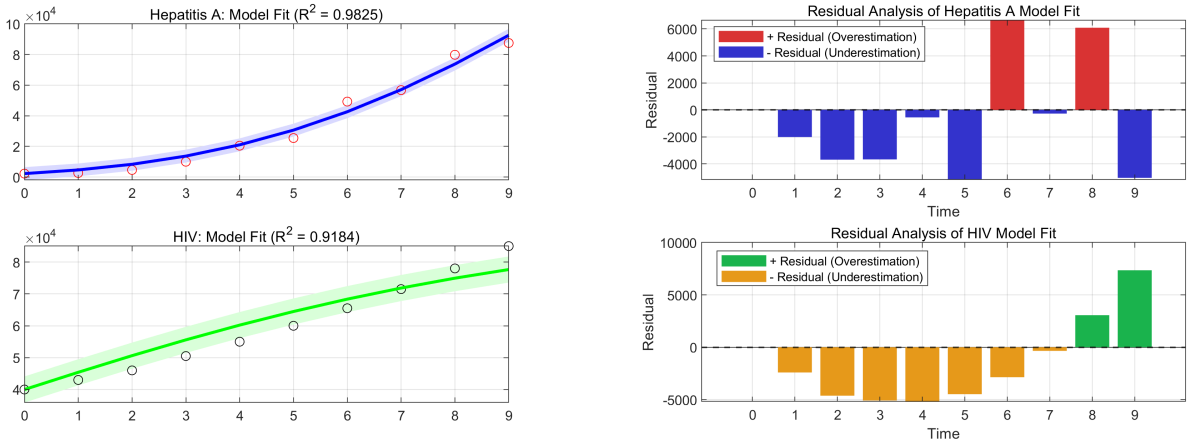

(a) Model fitting of co-infected model.

(b) Residual plots of fitted model.

Figure 5. Curve fitting and residual analysis of the model (2.9) with real U.S. HAV data and generated HIV data.

8. Numerical study

In this section, we utilized MATLAB's built-in routine bvp4c, a fourth-order collocation method, incorporating the framework (2.9), which coupled over time. This method would help us to understand the dynamics of disease deeply, and we would be able to know about the parameter that has a crucial effect on the model. Epidemiological researchers used numerous elements of data in the simulation, for instance, U.S. demographic data to represent scale, density, and population trends.

The model contains several repeating figures from the CDC-reported HAV incidence and the demographic records. On the other hand, since real HIV incidence data for the setting considered are not available, a synthetic HIV dataset was generated for the purpose of modeling and simulation. However, the initial values contain slightly smaller biologically reasonable assumptions. Numerous calculations give the model shape, outlining areas where demographic data turns to biological estimates and incidence changes to a simulation point. The initial conditions for the model are

$$S(0) = 322529932, \quad V(0) = 500000, \quad E(0) = 30000, \quad H_A(0) = 2245,$$

$$H_V(0) = 40000, \quad C(0) = 800, \quad T_V(0) = 12000, \quad R(0) = 400.$$

On the biological side, the decreasing infected patterns are positive signs of the successful intervention of the viral transmission. The decrease in co-infected people is an indication of the enhanced immune protection and reduction in exposure. This unification of all the compartments to balance is a symptom of the creation of the protection at the population level, as a result of vaccination and treatment and can be seen in Figure 6. As shown in Subfigure 6a, the susceptible population decreases sharply from about 3.2×10^8 to nearly 3.5×10^7, indicating rapid initial depletion followed by stabilization at a low level. As depicted in Subfigure 6b, the vaccinated population increases rapidly from 0 to approximately 2.9×10^8, with fast early growth that gradually slows toward saturation. As shown in Subfigure 6c, the exposed population increases monotonically from almost 0 to almost 2.0×10^6 with the growth rate decreasing after the mid-time. As observed in Subfigure 6d, the HAV-infected

population peaks around 4200 from an initial value near 2300, then declines steadily to below 500, indicating a rise-and-fall pattern. As shown in Subfigure 6e, the HIV-infected population increases from roughly 4×10^4 to about 9.4×10^4, with rapid early growth followed by a plateau. The number of co-infected people, shown in Subfigure 6f, also rises from about 800 to almost 9000, with a more rapid increase, especially after the mid-time. As illustrated in Subfigure 6g, the treated HIV population decreases gradually from around 12000 to nearly 6200, reflecting a steady decline over time. As observed in Subfigure 6h, the recovered population rises quickly to about 5.1×10^4 and then slightly declines to stabilize near 4.9×10^4.

Similarly, Figure 7 illustrates the collective impact of parameters α_A and α_V on all epidemiological classes. The reduction in the susceptible population signifies substantial depletion resulting from heightened transmission and vaccination, whereas the swift increase in the vaccinated group demonstrates effective coverage and impending saturation. The exposed and infected classes display maximum behavior indicative of active transmission at intermediate parameter values and a decline due to diminished susceptibility and the effects of interventions. The sharp decrease in H_V and T_V highlights the reduction in infection and treatment burden at higher rates. In contrast, the co-infected and recovered classes increase significantly, indicating enhanced disease progression dynamics alongside improved recovery. As shown in Subfigure 7a, the susceptible population S decreases from 1.9087×10^7 to 4.6962×10^6 with an increase of α_A and α_V, indicating strong depletion at larger values. In Subfigure 7b, the vaccinated population V increases rapidly with α_V, from 5.0950×10^6 to 2.4052×10^8, showing saturation behavior. In Subfigure 7c, the exposed population E rises at intermediate parameter values and then declines, varying between 2.4533×10^3 and 1.8598×10^7. In Subfigure 7d, the HIV-infected class H_A exhibits a peak, decreasing from 3.7474×10^6 to 4.5708×10^2. In Subfigure 7e, the class H_V decreases sharply with α_V, ranging from 4.63×10^6 to 9.21×10^7. In Subfigure 7f, the co-infection class C increases strongly with both parameters, from 8.73×10^3 to 1.69×10^8. In Subfigure 7g, the treated class T_V decreases with increasing α_V, varying between 1.46×10^5 and 2.55×10^6. Finally, in Subfigure 7h, the recovered class R increases significantly with both parameters, ranging from 1.50×10^4 to 1.94×10^8. Overall, this behavior emphasizes the critical role of maintaining high vaccination and treatment levels to control infection spread and promote recovery.

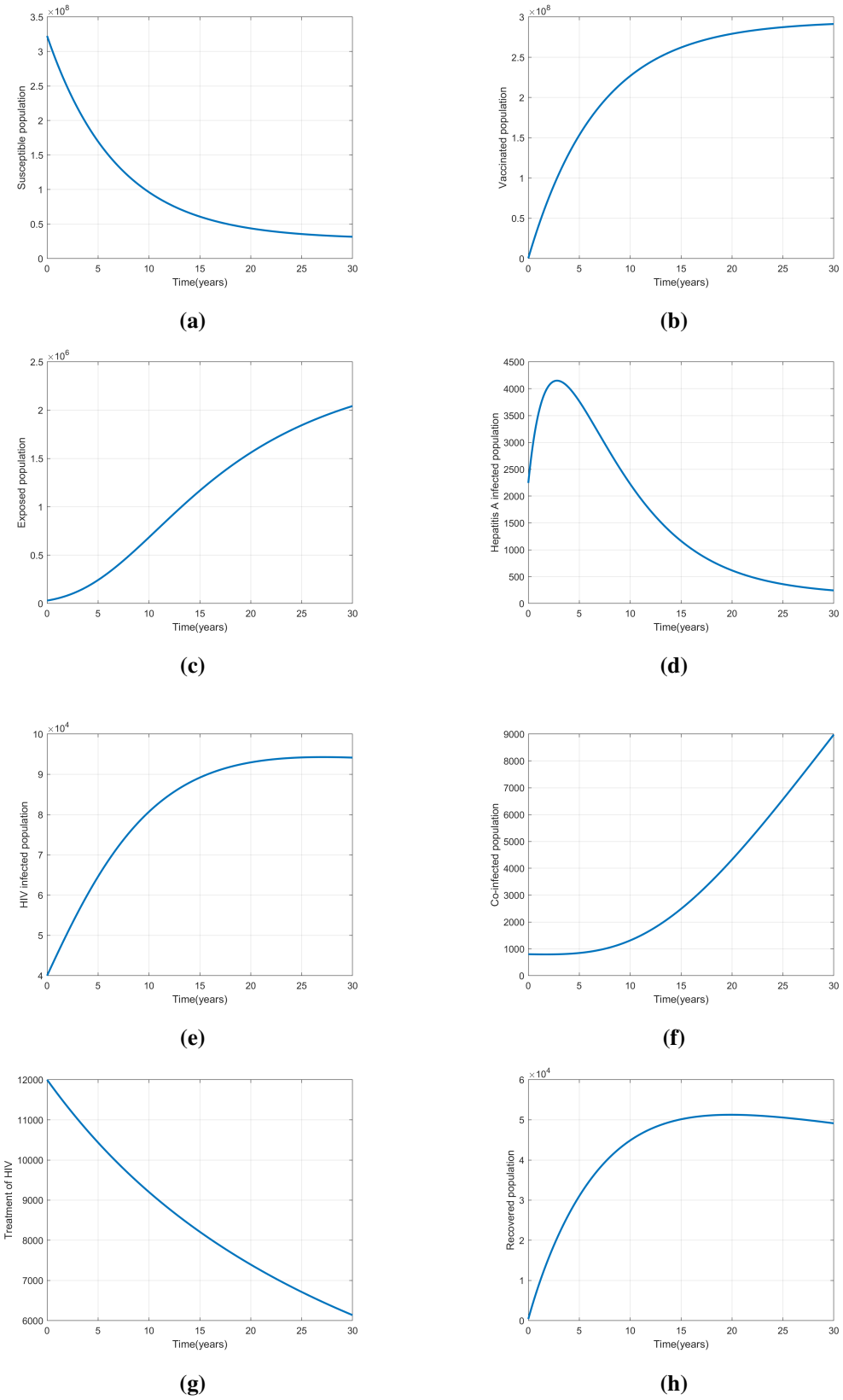

Figure 6. Time evolution of all compartments of model (2.9).

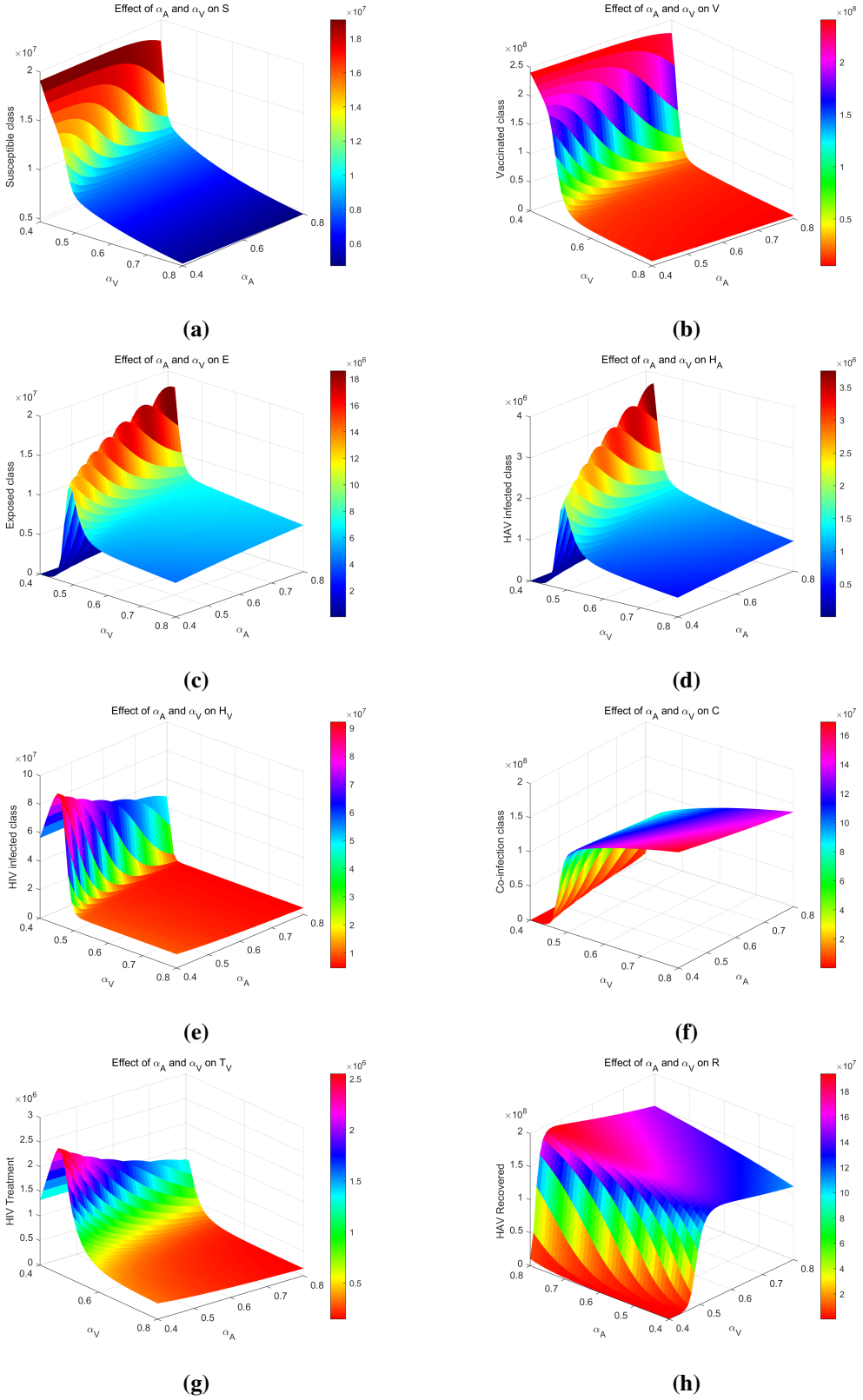

Figure 7. Surface plots of all compartments showing transmission rate effects.

8.1. Influence of key parameters on numerical dynamics

Numerical simulations were conducted to understand the effects of model parameters on the disease process through varying values of certain parameters of the process of transmission and control in the conditions of constant other values. Specifically, the rate of HIV transmission (α_A), HAV transmission (α_V), vaccination θ, and treatment progression rate (σ) were adjusted systematically.

When the transmission parameters α_V and α_A are increased, the epidemic peak and the time interval of the infected compartments increase, which means that there is stronger disease transmission. On the contrary, a higher rate of vaccination θ greatly decreases the exposed and HAV-infected population through a decrease of the susceptible pool. Likewise, the higher the treatment rate, (σ), the lower the HIV-infected and co-infected classes since it speeds up the movement into the treated compartment.

These simulations prove that transmission parameters enhance the epidemic transmission, whereas the vaccination and treatment parameters are inhibitory factors that can push the system to disease extinction in case they are large enough.

9. Simulation and results

Under this section, we discuss the numerical results generated by the model, which help reveal key relationships and the overall behavior of the system. The simulations offer a clearer picture of how important variables evolve over time, improving our understanding of the underlying dynamics. Comparing these results with real-world observations also helps validate the model, showing that it captures essential trends and can be reliably used to assess potential treatment strategies. Figure 6 illustrates the disease dynamics where an infected person spreads the infection to more than one other individual. In such a situation, the number of infections initially increases, reaches a peak, and then begins to decline as the vulnerable population shrinks, immunity builds up, or intervention measures begin to take effect. The simulation results as shown in Figure 7 indicate that increasing transmission-related parameters significantly alters population dynamics. There is a notable decrease in the susceptible class and a swift increase in both vaccinated and co-infected populations. The exposed and infected classes exhibit nonlinear behavior, showing peak values at intermediate parameter ranges, which suggests that certain transmission-related parameters can lead to complex interactions between these classes and influence overall disease spread. Computational studies also show that increasing HIV treatment availability and effectiveness significantly reduces the occurrence of new cases. These findings demonstrate the importance of successful treatment programs in restricting transmission, reducing additional infection levels, and moving the framework closer to disease-free status. Long-term sickness control and general sanitation improvement can be aided by improving and unifying treatment practices.

9.1. Extended discussion of simulation results

The graphical simulation allows one to gain a numerical understanding of how vaccination, transmission, and treatment interact. In our case, the populations of the infected first grow and attains the peak then stabilize slowly. The maximum of the outbreak is the most intense transmission and is connected with the inadequate control conditions. Transmission rates are of great importance in determining the magnitude and duration of this peak. For large values of the parameters, the system

exhibits saturation and transition effects, where the classes of recovery and co-infection are dominant and the classes of treated and vulnerable populations are reduced. The model demonstrates a notable sensitivity to transmission rates, emphasizing their crucial role in the propagation of disease and the outcomes of control measures.

The sensitivity analysis results indicate that even small changes in vaccination and treatment levels can lead to noticeable shifts in infection prevalence. This highlights how important it is to combine public health strategies, particularly vaccination and ART coverage, to effectively control the spread of infection.

10. Conclusions

This study explores the intricate relationship of HAV and HIV when both infections are present simultaneously in the host. It also incorporates a special compartment for those who have been vaccinated against HAV, allowing researchers to closely monitor vaccination effects in patients to understand the status of disease. The model provides valuable insights into managing co-infection transmission among vulnerable populations by quantifying the effect of vaccination in at-risk groups. Boundedness and nonnegativity were found to be important mathematical properties. The model's disease-free equilibrium points were found, giving important information about the stability of the system. The basic reproduction number was also calculated using the next-generation matrix method. We also performed the sensitivity analysis using LHS and PRCC methods. We aimed to reduce the parameters that most strongly influenced reproduction number in order to help lower the risk of infection in the population. The sensitivity analysis results indicate that α_V, σ, and θ are the most sensitive parameters, boosting the viral propagation. Local and global stability of the disease-free equilibrium was investigated through Routh–Hurwitz and Lyapunov methods, helping to identify the conditions under which the system remains stable. Model parameters were estimated using nonlinear curve fitting on real U.S. HAV data and synthetically generated HIV data, which helped confirm the model's accuracy in tracking disease trends. Numerical simulations were then run under various conditions to explore how changes in infection rates, transmission levels, and recovery rates influenced the population, using MATLAB for all computations. The results show that HAV vaccination and HIV treatment are effective in controlling viral spread and helping maintain viral control. MATLAB's built-in routine bvp4c, a fourth-order collocation method was used to numerically solve the epidemic model with improved accuracy and stability. This makes the method efficient for simulating long-term disease dynamics.

11. Limitations and future works

Studying HAV-HIV co-infection is tricky due to limited data, the complex ways the two viruses interact, and how the effectiveness of the HAV vaccine can vary, especially in people with weakened immune systems. The HAV-HIV co-infection model, developed by epidemiological researchers, is among the most complex disease structures globally. The scientists modeled the HAV-HIV co-infection due to their fascination with the way viral dynamics appear in overlapping populations. The study involves a full co-infection structure, and the absence of time-series data reflects the scientists' idea of the connection between clinical datasets and predictive reliability. The excellent and rigorous

research design contains various elements of science, such as parameters, datasets, and structure, as well as the principles of, for instance, precision and reliability. Because of the absence of publicly available longitudinal datasets for the co-infection of HAV and HIV, the calibration of the HIV part of the model was performed with synthetic data based on reported epidemiological trends. Hence, the quantitative predictions for co-infection burden should be looked at with caution. The incorporation of verified co-infection surveillance data will enable more stringent identifiability and model validation in the future. Additionally, the intricate dynamics of this particular co-infection make it difficult to understand the disease patterns. So, this co-infection needs more attention, and this could be overcome by incorporating ARTs and also by implementing the delay differential system of equations. This process is made more effective by introducing software focusing on R-programming, which is helpful in developing more comprehensive control measures that can improve treatment planning and overall health outcomes.

Author contributions

Shaiza Irum: Methodology, writing original draft, editing and writing review; Kashif Ali Khan: Methodology, writing original draft, editing and writing review, investigation, supervision; Nauman Raza: Methodology, writing original draft, formal analysis, software, editing and writing review, investigation, supervision; Waleed M. Abdelfattah: Editing and writing review, formal analysis, data curation; Wedad Albalawi: Formal analysis, software, editing and writing review, funding acquisition; Ahmed M. Shehata: Writing original draft, editing and writing review, data curation; Gamal M. Ismail: Methodology, writing original draft, editing and writing review, validation. All authors have read and approved the final version of the manuscript.

Use of Generative-AI tools declaration

The authors declare they have not used Artificial Intelligence (AI) tools in the creation of this article.

Acknowledgments

This work was supported by Princess Nourah bint Abdulrahman University Researchers Supporting Project number (PNURSP2026R157), Princess Nourah bint Abdulrahman University, Riyadh, Saudi Arabia. The authors are thankful to the Deanship of Graduate Studies and Scientific Research at University of Bisha for supporting this work through the Fast-Track Research Support Program. The authors extend their appreciation to the Deanship of Scientific Research, Islamic University of Madinah, Saudi Arabia for funding this research work.

Conflict of interest

The authors declare no conflicts of interest.

References

1. S. M. Lemon, Hepatitis A: Current view of an ancient disease, *J. Hepatol.*, **77** (2022), 243–244. https://doi.org/10.1016/j.jhep.2021.09.028
2. Z. Feng, S. M. Lemon, Hepatitis A virus, In: *The picornaviruses*, 2010, 383–396. https://doi.org/10.1128/9781555816698.ch24
3. O. Gholizadeh, S. Akbarzadeh, M. G. Hashemi, M. Gholami, P. Amini, Z. Yekanipour, et al., Hepatitis: Viral structure, classification, life cycle, clinical symptoms, diagnosis error, and vaccination, *Can. J. Infect. Dis. Med. Microbiol.*, **2023** (2023), 4263309. https://doi.org/10.1155/2023/4263309
4. H. E. Huang, O. Colasanti, T. F. Li, V. Lohmann, Limited impact of hepatitis A virus 3C protease-mediated cleavage on the functions of NEMO in human hepatocytes, *J. Virol.*, **99** (2025), e02264-24. https://doi.org/10.1128/jvi.02264-24
5. Centers for disease control and prevention, Hepatitis A. Available from: `https://www.cdc.gov/hepatitis-a/index.html`.
6. Wikipedia contributors, Hepatitis A. Available from: `https://en.wikipedia.org/wiki/Hepatitis_A`
7. Food & Wine, Most viral foodborne illnesses according to the World Health Organization. Available from: `https://www.foodandwine.com/most-viral-foodborne-illnesses-world-health-organization-8767812`
8. S. D. Lawn, S. T. Butera, T. M. Folks, Contribution of immune activation to the pathogenesis and transmission of human immunodeficiency virus type 1 infection, *Clin. Microbiol. Rev.*, **14** (2001), 753–777. https://doi.org/10.1128/cmr.14.4.753-777.2001
9. M. Haris, R. Abbas, Four decades of HIV: Global trends, testing assays, treatment, and challenges, *Zoonoses,*, **4** (2024), 997. https://doi.org/10.15212/ZOONOSES-2023-0039
10. S. Nyamweya, A. Hegedus, A. Jaye, S. Rowland-Jones, K. L. Flanagan, D. C. Macallan, Comparing HIV-1 and HIV-2 infection: Lessons for viral immunopathogenesis, *Rev. Med. Virol.* **23** (2013), 221–240. https://doi.org/10.1002/rmv.1739
11. R. D. Sloan, M. A. Wainberg, The role of unintegrated DNA in HIV infection, *Retrovirology*, **8** (2011), 52. https://doi.org/10.1186/1742-4690-8-52
12. N. Oliver, E. Chiao, Malignant diseases in HIV, In: *Fundamentals of HIV medicine: (CME edition)*, Oxford Academic, 2017, 351–338. https://doi.org/10.1093/med/9780190493097.003.0033
13. L. Lin, T. Li, Multidisciplinary collaborative integrated management of increasingly prominent HIV complications in the post-CART era, *HIV Med.*, **21** (2020), 683–691. https://doi.org/10.1111/hiv.13022
14. A. Turab, R. Shafqat, S. Muhammad, M. Shuaib, M. F. Khan, M. Kamal, Predictive modeling of hepatitis B viral dynamics: A Caputo derivative-based approach using artificial neural networks, *Sci. Rep.*, **14** (2024), 21853. https://doi.org/10.1038/s41598-024-70788-7

15. W. Sintunavarat, A. Turab, Mathematical analysis of an extended SEIR model of COVID-19 using the ABC-fractional operator, *Math. Comput. Simul.*, **198** (2022), 65–84. https://doi.org/10.1016/j.matcom.2022.02.009

16. H. Q. Zhang, B. Z. Cao, Q. T. Cao, M. Hun, L. Cao, M. Y. Zhao, An analysis of reported cases of hemophagocytic lymphohistiocytosis (HLH) after COVID-19 vaccination, *Hum. Vaccin. Immunother.*, **19** (2023), 2263229. https://doi.org/10.1080/21645515.2023.2263229

17. Y. Jia, B. Fu, L. Dong, M. Zhao, Sweet syndrome induced by SARS-CoV-2 vaccines: A systematic review of patient-report studies, *Hum. Vaccin. Immunother.*, **19** (2023), 2217076. https://doi.org/10.1080/21645515.2023.2217076

18. K. Xu, B. Gao, J. Li, Y. Xiang, L. Cao, M. Zhao, Clinical features, diagnosis, and management of COVID-19 vaccine-associated Vogt-Koyanagi-Harada disease, *Hum. Vaccin. Immunother.*, **19** (2023), 2220630. https://doi.org/10.1080/21645515.2023.2220630

19. J. Brown, K. Benedict, B. J. Park, G. R. Thompson III, Coccidioidomycosis: Epidemiology, *Clin. Epidemiol.*, **2013** (2013), 185–197. https://doi.org/10.2147/CLEP.S34434

20. World Health Organization, Chronic comorbidities & coinfections. Available from: https://www.who.int/teams/global-hiv-hepatitis-and-stis-programmes/hiv/treatment/chronic-comorbidities-and-coinfections

21. T. J. Nagu, M. Bakari, M. Matee, Hepatitis A, B and C viral co-infections among HIV-infected adults presenting for care and treatment at Muhimbili National Hospital in Dar es Salaam, Tanzania, *BMC Public Health*, **8** (2008), 416. https://doi.org/10.1186/1471-2458-8-416

22. I. Cropley, J. Main, Hepatitis C virus infection: co-infection with HIV and HBV, *Best Pract. Res. Clin. Gastroenterol.*, **14** (2000), 265–275. https://doi.org/10.1053/bega.1999.0075

23. I. Maier, G. Y. Wu, Hepatitis C and HIV co-infection: A review, *World J. Gastroenterol.*, **8** (2002), 577–579. http://dx.doi.org/10.3748/wjg.v8.i4.577

24. L. I. Backus, D. Boothroyd, L. R. Deyton, HIV, hepatitis C and HIV/hepatitis C virus co-infection in vulnerable populations, *AIDS*, **19** (2005), S13–S19. https://doi.org/10.1097/01.aids.0000192065.09281.01

25. E. A. Operskalski, A. Kovacs, HIV/HCV co-infection: Ppathogenesis, clinical complications, treatment, and new therapeutic technologies, *Curr. HIV/AIDS Rep.*, **8** (2011), 12–22. https://doi.org/10.1007/s11904-010-0071-3

26. Worldometer, United States population. Available from: https://www.worldometers.info/world-population/us-population/.

27. P. A. Naik, B. M. Yeolekar, S. Qureshi, M. Yeolekar, A. Madzvamuse, Modeling and analysis of the fractional-order epidemic model to investigate mutual influence in HIV/HCV co-infection, *Nonlinear Dyn.*,**112** (2024), 11679–11710. https://doi.org/10.1007/s11071-024-09653-1

28. P. van den Driessche, J. Watmough, Reproduction numbers and sub-threshold endemic equilibria for compartmental models of disease transmission, *Math. Biosci.*, **180** (2002), 29–48. https://doi.org/10.1016/S0025-5564(02)00108-6

29. J. C. Helton, F. J. Davis, Illustration of sampling-based methods for uncertainty and sensitivity analysis, *Risk Anal.*, **22** (2002), 591–622. https://doi.org/10.1111/0272-4332.00041

30. A. Ahmad, M. Farman, P. A. Naik, E. Hincal, E. Iqbal, Z. Huang, Bifurcation and theoretical analysis of a fractional-order hepatitis B epidemic model incorporating different chronic stages of infection, *J. Appl. Math. Comput.*, **71** (2025), 1543–1564. https://doi.org/10.1007/s12190-024-02301-2

31. J. P. LaSalle, *The stability of dynamical systems*, Philadelphia: SIAM, 1976.

32. Centers for Disease Control and Prevention, Hepatitis A surveillance 2020. Available from: `https://www.cdc.gov/hepatitis-surveillance-2020/about/index.html`.

AIMS Press